PHYSICAL REVIEW B VOLUME 27, NUMBER 12 15 JUNE 1983

Chemisorption of CO on Co(0001). Structure and electronic properties

F. Greuter,* D. Heskett, and E. W. Plummer
Department of Physics, University of Pennsylvania, Philadelphia, Pennsylvania 19104-3859

H.-J. Freund
Theoretical Chemistry Department, University of Köln, D-5000 Köln 41, West Germany
(Received 8 November 1982)

Angle-resolved photoemission with synchrotron radiation, low-energy electron diffraction, and x-ray photoelectron spectroscopy have been combined to study the behavior of chemisorbed CO on the hexagonal Co(0001) surface as a function of coverage, temperature, and CO partial pressure. The band structure was measured for the $(\sqrt{3}\times\sqrt{3})R30°$ (coverage $\Theta=\frac{1}{3}$ monolayer) and the $(2\sqrt{3}\times2\sqrt{3})R30°$ ($\Theta=\frac{7}{12}$ monolayer) phases. The results are compared to tight-binding calculations and show that hybridization effects for the 5σ and 1π bands and orbital mixing are important. The photoemission cross sections (shape resonances) are found to be significantly different for the high- and low-temperature phases.

I. INTRODUCTION

The chemisorption of CO on the cubic (fcc and bcc) group-VIII transition metals has been studied extensively in the past.[1] Much less work has been done on the hexagonal metals Co (Refs. 2–4) and Ru (Refs. 5 and 6), although they are known to be some of the most efficient catalysts for the reduction of CO by hydrogen.[6] In this and a paper planned for future publication we report on a detailed study of the interaction of CO molecules with the (0001) surface of cobalt by combining the surface techniques of low-energy electron diffraction (LEED), angle resolved and integrated uv photoemission, and x-ray photoelectron spectroscopy (XPS). Cobalt occupies a significant place in the periodic system between the well-studied metals Fe and Ni, on which CO adsorbs either dissociatively (Fe) or molecularly (Ni) at room temperature.[7] Furthermore, the (0001) surface of cobalt is hexagonal close packed, just as the (111) surface of a fcc structure. This allows a direct comparison to the corresponding fcc transition-metal surfaces where a number of structural phase transitions have been observed upon compressing the CO layer with increasing coverage.[6,8(a)–8(f)] In the present study we report on the related changes in the photoemission intensities and energies due to the lateral CO-CO interaction for adsorption at room temperature and at $\sim$170 K.

After a short description of the experimental procedure in the following section, we will discuss in Sec. III A the adsorption in the well-defined room-temperature phase and in III B we discuss the results for the incommensurate low-temperature phase. In Sec. IV we compare the experimental results to simple tight-binding calculations for an isolated, ordered CO layer. The Appendix contains data and analysis for the shape resonance in the photoionization cross section. A paper planned for future publication discusses the multielectron excitations in adsorbed CO compared to gas-phase CO and Co carbonyls.

II. EXPERIMENTAL PROCEDURE

The angle-resolved photoemission experiments were carried out at the Synchrotron Radiation Center of the University of Wisconsin. The polarized light from the storage ring was dispersed by a toroidal grating monochromator[9] and an angle-resolved hemispherical energy analyzer with an angular resolution of $\pm2.5°$ was used for detection of the photoemitted electrons.[10] The overall energy resolution was typically kept at $\sim$0.3 eV. The incoming photon flux was measured by a tungsten mesh photodiode. The base pressure was kept below 2×10^{-10} Torr by using an ion pump and a liquid-nitrogen-cooled Ti sublimator. The sample was mounted on a two axis of rotation manipulator, which allowed cooling down to $\sim$170 K and heating to 700 K or higher. A similar sample mount was used for the angle integrated ($\pm6°$ collection angle) uv- and x-ray photoemission experiments, which were done on a VG ESCALAB 5, equipped with a four-grid LEED optics, a uv-resonance lamp, and a

twin Mg/Al anode. The latter system is pumped by diffusion pumps and a Ti sublimator, with a base pressure below 1×10^{-10} Torr routinely obtained. The crystal was obtained cut, polished, and oriented to within 1° of the (0001) axis from the Cornell Materials Science Center in Ithaca, New York. Carbon and oxygen were found to be the main contaminants. Initial cleaning of the crystal was accomplished by many cycles of Ar (or Ne) ion bombardment and annealing at 350–400 °C. Care was taken to stay below the hcp-fcc phase transition at ~400 °C.[2]

It was found that oxygen adsorption at room temperature and subsequent heating to $\lesssim$400 °C is very efficient in depleting the surface region of carbon, which segregates from the bulk. Surface oxygen, on the other hand, can be removed by heating in hydrogen or adsorbing CO at room temperature and subsequent flashing to ~250 °C. After a prolonged cleaning procedure it was sufficient to use a mild sputtering followed by annealing at ~350 °C for ~20 min.

The cleanliness of the surfaces was monitored either with XPS or judged from the intensity of the Λ_1-surface state[11] while doing the angle-resolved photoemission experiments. It was found that this surface state stayed unaffected for 1–2 h under our vacuum conditions at room temperature, but is immediately quenched by adsorption of CO or hydrogen. The in-plane orientation of the crystal was determined in a first step by LEED, which showed a well-ordered hexagonal pattern, and then more precisely by using angle-resolved photoemission.

III. EXPERIMENTAL RESULTS

A. Adsorption at room temperature

A saturation exposure of <10 L (1 L=1 langmuir$=10^{-6}$ Torr sec) CO at room temperature produces a clear $(\sqrt{3}\times\sqrt{3})R30°$ LEED pattern on the Co(0001) surface. This structure is observed on all hexagonal transition-metal surfaces[6,8] and has been reported for Co before.[2,4] The CO molecules form a hexagonal overlayer with a coverage corresponding to $\Theta=\frac{1}{3}$ monolayer (ML) and a nearest-neighbor distance of 4.35 Å as illustrated in Fig. 1(a). All the molecules occupy the same lattice site, although the site is not yet known for cobalt. Possible bonding sites are the two threefold hollow sites as for Ni(111) or Pd(111), but these are not always the energetically most favorable places as the examples of Pt(111) and Cu(111) show, where the on-top site seems to be preferred (see compilation in Ref. 12). Upon CO adsorption at room temperature we observe a work function increase of 0.75 ± 0.1 eV (clean work function: 5.1 ± 0.1 eV), which is slightly higher than the value of $+0.65$ eV reported by Papp[4] for the maximum LEED intensity of the $(\sqrt{3}\times\sqrt{3})R30°$ structure for adsorption at 100 K.

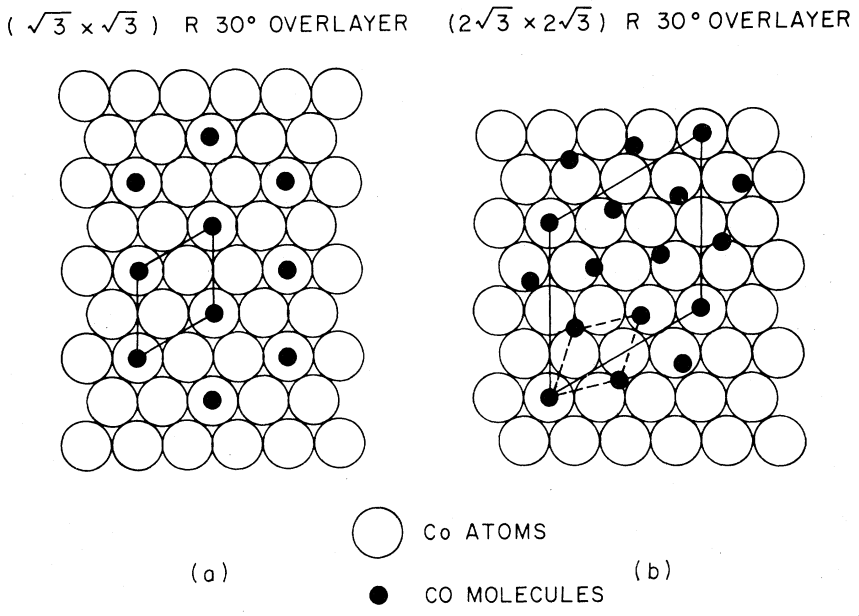

FIG. 1. (a) Co(0001) surface (open circles) with a $(\sqrt{3}\times\sqrt{3})R30°$ CO overlayer (solid circles), $\Theta=\frac{1}{3}$ ML. Note that the actual bonding site is not known. (b) Overlayer structure for the incommensurate $(2\sqrt{3}\times2\sqrt{3})R30°$ phase with $\Theta=\frac{7}{12}$ ML. (The position of the coincidence lattice is again unknown.)

Figure 2 shows photoemission spectra for the room-temperature phase for three different collection geometries. Based on the known symmetry of the molecular-ion states the orientation of the molecular axis with respect to the surface can be determined.[1] The two adsorbate-induced peaks at -10.7 and -7.9 eV in Fig. 2(a) are readily assigned to the 4σ and the almost degenerate 5σ and 1π ion states, just as observed in most other CO adsorption studies.[1] The bonding of CO to the transition metal is the result of donation from the CO 5σ level to the substrate and a metal to CO back donation into the empty CO 2π orbital as discussed in the literature (see references in Ref. 1). In this simple picture the bonding is mainly done by the 5σ orbital, which has most of its amplitude on the carbon atom and undergoes a shift of ~ 3 eV toward the 1π and 4σ levels due to the formation of the CO—substrate bond.

The orientation of the molecules can be obtained by using symmetry selection rules and the polarized light of the synchrotron, as is illustrated in Figs. 2(b) and 2(c). The light is set at normal incidence; the polarization vector $\vec{A}$ therefore lies in the plane of the surface and electrons are collected in a mirror plane of the crystal with the $\vec{A}$ vector either parallel [Fig. 2(b)] or perpendicular [Fig. 2(c)] to the collection plane. These are usually referred to as the "allowed" or "forbidden" geometries since a state with even symmetry with respect to the collection plane has a vanishing dipole matrix element for the forbidden geometry.[1] The almost complete disappearance of the 4σ level in the forbidden geometry of Fig. 2(c) proved that CO prefers to bond perpendicular to the (0001) surface as it does on most other transition metals studied so far. The incomplete suppression of the 4σ intensity in Fig. 2(c) can be explained by the incomplete polarization of the light, the finite angular resolution, an uncertainty ($\pm 1.5°$) in the alignment of the crystal, and the possible presence of crystal defects, as well as a possible thermal fluctuation of the bond angle. The peak at -7.7 ± 0.2 eV in Fig. 2(c) is due to the emission from the odd π orbital plus a small contribution from the incompletely suppressed 5σ orbital.

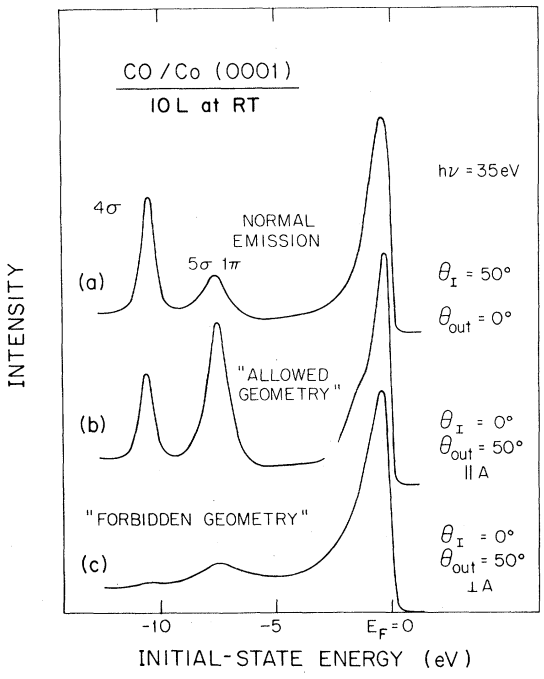

FIG. 2. Typical spectra for saturation coverage at room temperature (RT) for p-polarized light and normal emission (a) and s-polarized light with the polarization vector $\vec{A}$ parallel (b) or perpendicular (c) to the collection plane, which was the $\bar{\Gamma}\bar{K}$ mirror plane.

Further evidence for a perpendicular orientation of the molecules comes from the observation of the shape resonance in the 4σ and 5σ-1π cross sections. At resonance the emission is strongly peaked near the molecular axis. In the present experiment this peaking was observed along the surface normal, as we will discuss later (see Appendix). Taking these facts together we find that the CO molecules adsorb molecularly on Co(0001) at room temperature with the molecular axis along the surface normal with the carbon end down. Essentially the same behavior was found for adsorption at 170 K except for the significant changes in the shape resonance, as discussed in the Appendix. No signs of dissociation were observed for the (0001) surface under normal conditions, in agreement with other findings.[2–4] Prior *et al.*[13] and Papp,[4] however, report dissociative adsorption above room temperature for the higher indexed $(10\bar{1}2)$ and $(11\bar{2}0)$ surfaces. Extended LEED or ultraviolet photoelectron spectroscopy (UPS) work at high CO pressures ($\sim 1\times 10^{-5}$ Torr) showed in the present experiment a weak carbon and oxygen buildup on the (0001) surface as well.

The interaction among the CO molecules in the well-ordered $(\sqrt{3}\times\sqrt{3})R30°$ room-temperature phase is strong enough to form a two-dimensional band structure for the overlayer. Such a band formation has been observed before for CO adsorption on Ni(100),[14] Pd(100),[15], Fe(110),[16] and Ir(111).[17] The band dispersion can be directly mapped out by means of angle-resolved photoemission, where the relation between the surface reciprocal wave vector $k_{||}$ and the quantities measured in the experiment is

$$k_{||}=(2m_e\hbar^{-2}\epsilon)^{1/2}\sin\theta$$

where θ is the collection angle with respect to the surface normal and kinetic energy $\epsilon=h\nu-\epsilon_b-\phi$,

with ϵ_b the binding energy and ϕ the work function. The results are summarized in Fig. 3 for the two symmetry directions $\bar{\Gamma}\bar{M}$ and $\bar{\Gamma}\bar{K}$ of the surface Brillouin zone and have been reported before in a short paper.[18] Most of the data has been collected with p-polarized light at an angle of incidence of $\theta_I = 50°$ and for photon energies of 30–40 eV, where the 5σ contribution to the unresolved 5σ-1π emission is dominant. The dispersion of the 4σ and 5σ bands behave qualitatively as expected. Bands derived from σ orbitals should have minima at $\bar{\Gamma}$ and maxima at $\bar{K}$ or $\bar{M}$ while the behavior of the σ-derived bands is reversed. A simple analysis of this dispersion behavior will be given in Sec. IV. Along the $\bar{\Gamma}\bar{K}$ direction the dispersion flattens out at large $k_{||}$ since we follow the line $\bar{K}\bar{M}\bar{K}$ in the second surface Brillouin zone. Along the $\bar{\Gamma}\bar{M}\bar{\Gamma}$ direction the 4σ dispersion is periodic about the $\bar{M}$ point returning to the value of $\bar{\Gamma}$ in the second zone. This is not clear for the 5σ-1π dispersion where at large collection angles (i.e., large $k_{||}$) the emission from the 1π orbitals becomes more important,[1,19] as we can see from the increase in the linewidth. This results in a slight upwards shift of the combined 5σ-1π peak position and explains the observed deviation from the expected behavior as we penetrate the second zone (along $\bar{\Gamma}\bar{M}\bar{\Gamma}$). Some data points ($\times$'s) for the odd 1π band obtained in the forbidden geometry are shown as well in Fig. 3 for $k_{||}$ along $\bar{K}\bar{M}\bar{K}$. Extending the measurements to larger values for $k_{||}$ (i.e., higher photon energies) would, in principle, allow one to map the odd π band in the third zone and hence to obtain the missing dispersion around $\bar{\Gamma}$.

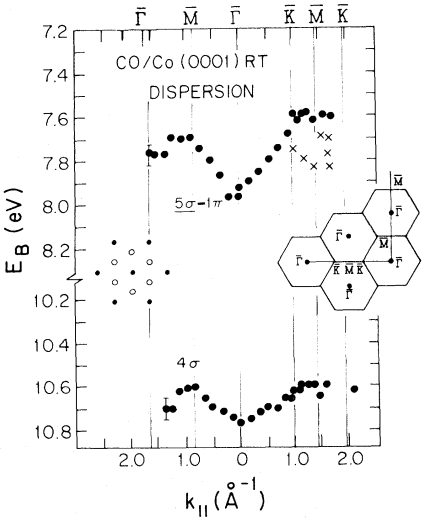

FIG. 3. Measured 4σ(●), 5σ-1π(●), and odd 1π($\times$) dispersion for the $(\sqrt{3}\times\sqrt{3})R\,30°$ structure. The extended surface Brillouin zone and the observed LEED pattern are shown as insets.

The overall bandwidth in the saturated room-temperature phase is 0.15 ± 0.05 eV for the 4σ band and 0.35 ± 0.05 eV for the 5σ and 1π bands, as can be seen from Fig. 3. A word of caution is appropriate here about the determination of the molecular level sequence[3,4] for a system with band formation. The orbital sequence can be a strong function of $k_{||}$, as is evident from Fig. 3. Further care is appropriate if there is a tendency for island formation at low coverage, as in the present case (see Sec. III B).

Thermal desorption spectra for the room-temperature phase show a single desorption peak at $\sim 160\,°C$,[2] in agreement with the picture of a single type of adsorption site. Adsorbing more CO than necessary to produce a $(\sqrt{3}\times\sqrt{3})R\,30°$ structure at room temperature does not cause a change in the LEED pattern, in agreement with Bridge *et al.*[2] At a standing CO pressure of $p_{CO} > 5\times10^{-9}$ Torr, however, the overlayer spots were observed[2] to become diffuse and started to split. This indicates the onset of the formation of a new overlayer structure, which Bridge *et al.*[2] tentatively assigned to a $(\sqrt{7}\times\sqrt{7})R\,19.2°$ structure with $\Theta = \frac{4}{7}$ ML. At the same time the thermal desorption spectrum[2] shows a shoulder on the low temperature side of the main peak. Both these observations indicate a compression of the commensurate room-temperature phase to a denser packed phase, but a detailed understanding of the thermal desorption spectrum for this phase must include the effects of the structural relaxation in the compressed CO layer during the desorption process.

In the "angle-integrated" photoemission experiments we observe a ~ 0.1 eV shift for the σ levels to higher binding energy and a work-function increase of ~ 0.2 eV at room temperature if the CO pressure is held at 1×10^{-6} Torr. The compressed phase converts immediately back to the stable $(\sqrt{3}\times\sqrt{3})R\,30°$ structure whenever the CO is pumped out of the chamber. This is in agreement with the measured heat of adsorption, which drops by $\sim 25\%$ as the coverage is increased above $\Theta = \frac{1}{3}$ ML. Of course it is very likely that further phase transitions can be found at different places in the P-T phase diagram for CO/Co(0001).

Upon cooling the substrate some of the compressed phases can be obtained as stable phases even at zero CO partial pressure for most of the hexagonal transition-metal surfaces.[8] The size of the substrate lattice spacing thereby plays a crucial role in deciding which overlayer structures are possible. The CO-CO repulsion sets a lower limit for the nearest-neighbor distance, which seems to be of the order of ~ 3.3 Å.[4,8(a),8(f)]

B. Adsorption at low temperatures (~ 170 K)

At low coverage (~ 1 L) a sharp $(\sqrt{3}\times\sqrt{3})R30°$ LEED pattern is observed as the first ordered low-temperature phase. With increasing CO exposure this pattern becomes weak and diffuse and suddenly develops into a sharp $(2\sqrt{3}\times 2\sqrt{3})R30°$ structure, as first reported by Papp[4] for adsorption at 100 K. This is the only observed ordered high-coverage—low-temperature phase. In the present study we did find the same structure for saturation coverage at a higher temperature of 170 K. The LEED pattern (see inset in Fig. 4) is very similar to the one reported by Comrie and Weinberg[8(a)] for the saturated Ir(111) surface at 250 K and the one observed by Williams and Weinberg[6] for Ru(0001) at 110 K. In the latter case this was not yet the saturated low-temperature phase due to the larger lattice spacing ($a=2.70$ Å) for Ru compared to ($a=2.51$ Å) Co (Ir: $a=2.71$ Å). Assuming a perfect hexagonal array of molecules, the nearest-neighbor distance for the $2\sqrt{3}$ structure turns out to be 3.29 Å for Co and the coverage $\Theta=\frac{7}{12}$ ML. The resulting incommensurate overlayer structure is schematically shown in Fig. 1(b). Interestingly enough the same $2\sqrt{3}$ structure has not been found for the Ni(111) surface, where the substrate lattice spacing is smaller by only 0.8% compared to Co. A saturated Ni(111) surface shows a $(\sqrt{7}/2\times\sqrt{7}/2)R19.1°$ overlayer at 200 K and a corresponding coverage of $\Theta=\frac{4}{7}$ ML, which is only 2% less than for the $2\sqrt{3}$ structure.[4,8(e)] No denser structures could be observed on Co, not even with a standing CO pressure of 1×10^{-5} Torr at 170 K. At 10^{-10} Torr the LEED pattern disappeared within ~ 30 sec under the influence of the electron beam, but came back at a standing CO pressure of $>1\times10^{-7}$ Torr. No signs of dissociation were observed for a short exposure of the overlayer to the electron beam, indicating that desorption rather than dissociation takes place. After an extended operation time at high CO pressure, however, it was no longer possible to get the $2\sqrt{3}$ structure and a $(\sqrt{7}/3\times\sqrt{7}/3)R10.9°$ LEED pattern was observed instead, corresponding to $\Theta=\frac{3}{7}$ ML. At the same time the XPS showed an increase in the C 1s signal, indicating the blocking of certain sites by carbon atoms.

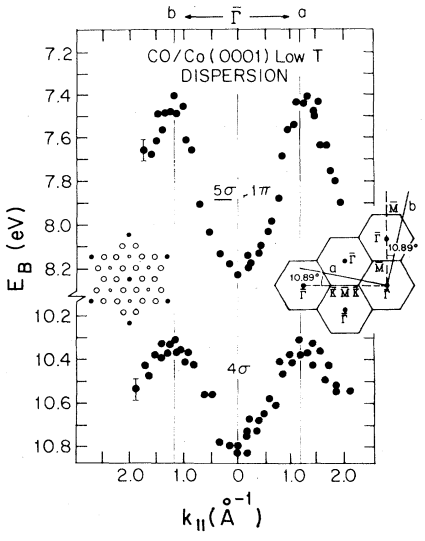

FIG. 4. Dispersion of the 4σ, and 5σ and 1π bands for the $(2\sqrt{3}\times 2\sqrt{3})R30°$ overlayer. The probed direction in the surface Brillouin zone (solid lines) and the observed LEED pattern are shown as insets.

The photoemission data for the low-temperature phase were collected at 170 K and saturation coverage. The directions probed in $k_{||}$ space are $\bar{\Gamma}\bar{M}\bar{\Gamma}$ and $\bar{\Gamma}\bar{K}\bar{M}\bar{K}$ of the Brillouin zone of the clean surface. The primitive unit cell of the $(2\sqrt{3}\times 2\sqrt{3})R30°$ structure is rotated by 10.9° with respect to the primitive unit cell of the clean surface (the nonprimitive $2\sqrt{3}$ unit cell with 7 molecules per cell described the coincidence lattice of adsorbate and substrate). This means that we actually probe the CO overlayer along two perpendicular directions in $k_{||}$ space, rotated by 10.9° from the main symmetry directions $\bar{\Gamma}\bar{M}$ and $\bar{\Gamma}\bar{K}\bar{M}$ of the isolated CO layer, as is shown in the inset of Fig. 4. Two domains are possible for this structure.[17]

Figure 5 shows a set of photoemission spectra for the low-temperature phase for various photon energies and polar angles of collection and illustrates the dispersion of the 4σ, 5σ, and 1π bands. The data were again collected with p-polarized light in the photon-energy range where the 5σ emission is strongest (see Appendix). The contribution from the 1π band can be seen as a pronounced shoulder in certain geometries in Fig. 5. The measured dispersion is summarized in Fig. 4. From the comparison of Figs. 3 and 4 it is obvious that the denser packing of the CO in the low-temperature phase results in an increase of the width of all bands. The nearest-neighbor distance decreases from 4.35 Å at room temperature to 3.29 Å for the $2\sqrt{3}$ structure, resulting in an increase in the 4σ bandwidth from 0.15 to 0.48 ± 0.05 eV. Qualitatively the same observation is made for the 5σ band (increase from 0.3 to 0.8 eV), although hybridization effects with the 1π bands are quite important, as we will discuss later.

In Fig. 4 the bands are observed to turn around at a larger $k_{||}$ than for the $(\sqrt{3}\times\sqrt{3})R30°$ structure, in agreement with the reduced lattice spacing in real space. The expected zone-boundary crossings for the $2\sqrt{3}$ structure are shown in Fig. 4 by the vertical lines and agree with the data within the experimen-

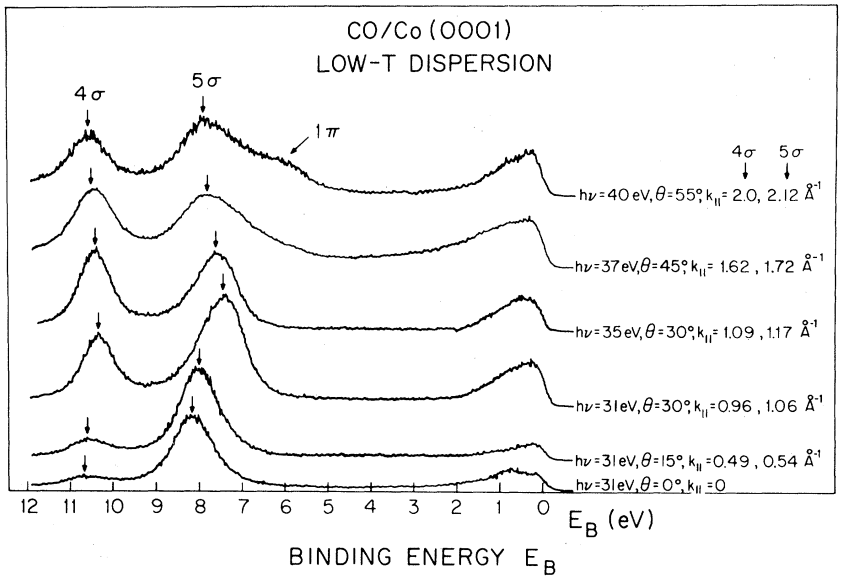

FIG. 5. Spectra illustrating the dispersion found for a saturated CO overlayer at 170 K ($k_{||}$ is along line *a* in Fig. 4).

tal uncertainties. The dispersion is not symmetric about these zone boundaries since we penetrate the second surface Brillouin zone along nonsymmetric lines (see inset of Fig. 4).

Mapping out the dispersion of the π bands is in general quite difficult and we will only discuss here their behavior at $\bar{\Gamma}$, the center of the surface Brillouin zone. For normal emission ($k_{||}=0$) transitions from all orbitals are symmetry allowed for *p*-polarized light. The emission from the σ orbitals, however, can be significantly suppressed by going to low photon energies ($h\nu \lesssim 25$ eV), where the cross section is small relative to the 1π, and/or by using *s*-polarized light, since the σ intensity scales with the square of the electric field component A_z perpendicular to the surface (see Refs. 1, 19 and 20). This allows us to estimate and separate the contribution from the 5σ orbital to the overlapping 5σ and 1π peaks, as is illustrated in Figs. 6 and 7.

Figure 6 shows spectra taken in normal emission as a function of exposure at 170 K for nearly normally incident light (almost *s* polarized). For low exposures ($\lesssim 2$ L) only the 5σ-1π peak can be resolved clearly at -7.5 ± 0.1 eV. The 4σ emission is rather weak in this geometry and at this photon energy. By analyzing the normal emission data over the photon-energy range $h\nu=25$–40 eV, we can identify the 1π level at $\bar{\Gamma}$ at -7.25 ± 0.3 eV and the 5σ and 4σ orbitals at -7.9 ± 0.1 eV and -10.75 ± 0.05 eV, respectively. The latter values are within the given uncertainty identical to those for the saturated room-temperature phase. Below 2 L no coverage dependence of the peak positions and only an exposure-dependent intensity increase are observed. This indicates the growth of islands of $(\sqrt{3}\times\sqrt{3})R30°$ structure, in agreement with the LEED observations.[4] Increasing the exposure to a total of 5 L results in a splitting of the 5σ-1π peak

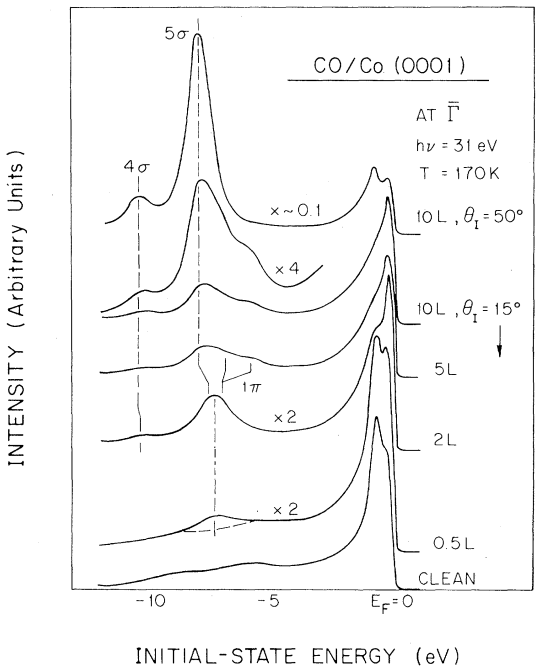

FIG. 6. Coverage dependence for CO adsorption at 170 K. These spectra are for normal emission with the parallel component of $\vec{A}$ in the $\bar{\Gamma}\bar{K}$ direction of the clean surface.

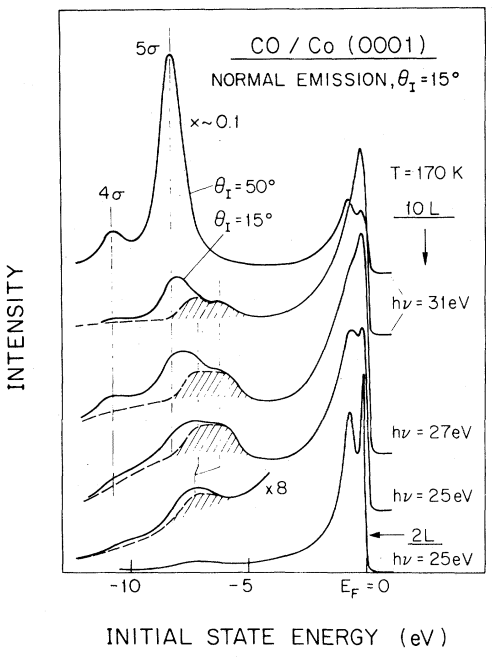

FIG. 7. Tentative separation of the 5σ and 1π emission at the center $\bar{\Gamma}$ of the surface Brillouin zone. The 1π contribution is shown as the shaded area for both the $(\sqrt{3}\times\sqrt{3})R\,30°$ (2 L) and the $(2\sqrt{3}\times 2\sqrt{3})R\,30°$ (10 L) overlayers.

(in normal emission) as seen in Fig. 6. The 4σ and 5σ levels at $\bar{\Gamma}$ are lowered in energy while the 1π level is pushed up toward the Fermi level. Further CO exposure does not influence the peak positions and increases the intensity of the CO features by only a few percent. Angle-integrated measurements at low temperatures with a CO partial pressure of 1×10^{-5} Torr did not show any changes, indicating that this phase cannot be compressed any further. The room-temperature phase, on the other hand, can be compressed, as mentioned above. This agrees with our observation that the HeI spectra at room temperature and a high CO pressure resemble those of the saturated low-temperature phase and are characterized by a 1π-derived shoulder at the low-binding-energy side of the 5σ-1π peak for nearly normal collection.

Spectra for the saturated low-temperature phase at $\bar{\Gamma}$ have been measured for light incident at $\theta_I = 15°$, 20°, and 50° and the observed strong angular dependence of the σ emission is illustrated at the top of Fig. 7. This angular dependence can be estimated[20] and we can subtract out the 5σ contribution to the spectra taken at $\theta_I = 15°$. The remaining π contribution is shown in Fig. 7 by the shaded area. In the saturated low-temperature phase we find the π bands at $\bar{\Gamma}$ centered at 6.6 ± 0.3 eV binding energy. The unusual line shape indicates split π bands at $\bar{\Gamma}$. This splitting of the π bands is rather surprising, since in an isolated hexagonal CO layer the two π bands must be degenerate at $\bar{\Gamma}$ due to the high symmetry (C_{6v}) of this point. The observed splitting, therefore, means that in the low-temperature phase the relevant symmetry is lowered (lower than C_{3v}) and the degeneracy of the π bands at $\bar{\Gamma}$ removed. This could be due either solely to a lowering of the symmetry by including the incommensurate substrate or to a possible structural deformation of the overlayer under the stress introduced by the incommensurate substrate. At best only one out of seven CO molecules occupies a high-symmetry lattice site for a perfect hexagonal array in the $2\sqrt{3}$ structure.[4,6,8] Most of the molecules, however, are very close to a symmetric site (within $\sim5-10\%$ of their nearest-neighbor distance) and it might be energetically favorable to slightly distort the overlayer lattice toward these sites, without changing the $(2\sqrt{3}\times2\sqrt{3})R\,30°$ coincidence lattice. Pritchard[8(d)] did show by optical-simulation techniques that such small distortions are difficult to distinguish by LEED. The effect on the band dispersion in the present experiment would be to smear out the location of the zone boundaries and it seems reasonable to assume that, due to their relatively large spatial extent, the π orbitals are most sensitive to these short-range distortions. We will discuss these points in some more detail in the following section and only mention here that it certainly goes beyond the present experiment to deduce a model for a possible distorted local structure. Table I summarizes the binding energies and bandwidths observed for the two different ordered phases of CO on Co(0001). We will compare this experimental data to theoretical calculations in Sec. IV.

To conclude this section we briefly discuss the strong changes observed for the metal d bands upon CO adsorption as is evident from Figs. 6 and 8. The surface electronic structure at $\bar{\Gamma}$ of clean Co is characterized by an sp-like surface state at 0.3 eV binding energy.[11] Owing to its Δ_1 symmetry (Λ_1 in fcc notation[11]), this surface state is seen only with p-polarized light and its emission is strongest at low photon energies. Adsorption of CO or hydrogen quenches this state as is evident from Fig. 8. Transitions from bulk states are also significantly affected by CO adsorption. This is shown in Fig. 6, where the emission from the surface state is suppressed by the almost complete s polarization of the light and the high photon energy.[11] The overall d-band intensity decreases upon CO adsorption and the higher-binding-energy peak at -0.7 ± 0.1 eV, which represents transitions from the Δ_6 minority-spin band,[11] disappears almost completely. Two effects

TABLE I. Binding energies and bandwidths of CO-derived energy levels.

CO structure	CO-CO spacing	Work function	Binding energies with respect to E_F					Bandwidth ratios	
			4σ at $\bar{\Gamma}$	$\bar{\Gamma}\rightarrow\bar{K}$	5σ at $\bar{\Gamma}$	$\bar{\Gamma}\rightarrow\bar{K}$[a]	1π at $\bar{\Gamma}$	$\bar{\Gamma}\rightarrow\bar{K}$[a]	5σ:4σ	1π:4σ
					Experiment					
$(\sqrt{3}\times\sqrt{3})R30°$	4.35 Å	5.85±0.2	10.75±0.05	0.15±0.05	7.9±0.1	0.35±0.05	7.25±0.3	0.35	2.3±1	2.3
$(2\sqrt{3}\times2\sqrt{3})R30°$	3.29 Å	6.2 ±0.2	10.82±0.05	0.48±0.05	8.2±0.05	0.8 ±0.05	6.6 ±0.3[b]	1.1	1.7–2.0°±0.3	2.3–1.9[c]
					Theory: Gas-phase CO with no σ-π interaction [Fig. 10(a)]					
Hexagonal	4.35 Å			0.14		0.36		0.37	2.6	2.6
Hexagonal	3.29 Å			0.62		1.63		1.58	2.6	2.5
					Theory: Gas-phase CO with σ-π interaction [Fig. 10(c)]					
Hexagonal	4.35 Å			0.14		0.23		0.37	1.6	2.6
Hexagonal	3.29 Å			0.62		1.02		1.58	1.6	2.5

[a] The bandwidth measured for the 5σ and 1π bands included hybridization. In both cases the energy given is from the appropriate Γ point to the K_3 point (Figs. 12 and 13).

[b] This π level is split at $\bar{\Gamma}$ by 1.1 eV (see Fig. 7).

[c] Estimated effect due to 10° misalignment of structure.

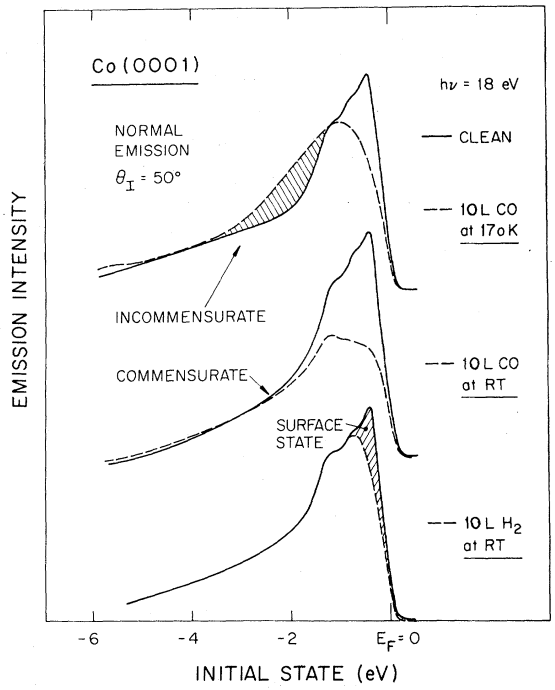

FIG. 8. Modification of the *d*-band emission at $\bar{\Gamma}$ for a commensurate or incommensurate CO overlayer and after chemisorption of H_2.

may contribute to this behavior: First, the bonding of CO to the metal changes the character of the substrate wave functions in the surface region and hence the photoemission matrix element, and second, the presence of the overlayer creates an extra scattering source for the outgoing final-state wave function at the metal-vacuum interface. The latter effect might be particularly important for an incommensurate overlayer, as the comparison of the room- and low-temperature spectra in Fig. 8 (or the spectra for >2 L exposure in Fig. 6) indicates. Hence care must be taken not to assign such effects to metal-CO backdonation, for which we did not find any clear evidence throughout the experiment.

IV. TIGHT-BINDING LINEAR COMBINATION OF MOLECULAR ORBITALS (LCMO) CALCULATIONS OF DISPERSION

In order to achieve a qualitative understanding of the experimental results presented in Sec. III we have carried out tight-binding calculations,[21] assuming only nearest-neighbor interactions with *ab initio*[22] wave functions and semiempirical CNDO-type (where CNDO means complete neglect of differential overlap) wave functions[23] to determine the intermolecular interaction parameters. The matrix elements of the Hamiltonian H can be written as

$$H_{ij}(\vec{K})=N\sum_{\vec{n}} e^{i\vec{K}\cdot R\vec{n}}A_{ij}(\vec{n}) , \quad (1)$$

where

$$A_{ij}(\vec{n})=\langle \psi_i(\vec{r}-R\vec{n}) \mid H \mid \psi_j(\vec{r})\rangle \quad (2)$$

using the molecular-orbital wave functions $\psi(\vec{r})$ of CO as basis functions. The matrix R determines the position of the molecules in real space, with $\vec{n}=(n_1,n_2)$ being the two-dimensional Miller indices. Since we are only interested in the dispersion of the CO bands we have chosen to set the matrix elements $A_{ij}(\vec{n})$ to be proportional to the overlap between the basis functions $\psi_i(\vec{r})$ and $\psi_j(\vec{r})$ centered at different positions in real space:

$$\langle \psi_i(\vec{r}-R\vec{n}) \mid H \mid \psi_j(\vec{r})\rangle \simeq K\langle \psi_i(\vec{r}-R\vec{n}) \mid \psi_j(\vec{r})\rangle = KS_{ij} . \quad (3)$$

The proportionality factor is represented by the matrix $(K_{\mu\nu})$, where μ and ν are the indices of atomic orbitals that have been used to describe the molecular wave functions as a linear combination of atomic orbitals (LCAO) function. For each type of atomic orbital, i.e., s, p, or d functions, a $K_{\mu\nu}$ has to be determined. The simplest choice is to take the matrix element from textbooks on semiempirical calculations where these values are tabulated.[23] We have chosen the values used in the CNDO method, where the values of $K_{\mu\nu}$ do not depend on the atomic expansion coefficients of the molecular-orbital wave functions. Another way to determine interaction matrix elements is to do a self-consistent Hartree-Fock calculation for a pair of CO molecules and look for the orbital splitting of equivalent orbitals. This procedure has the pronounced disadvantage that the interaction matrix elements have to be determined separately by self-consistent-field (SCF) calculations for each separation of the molecules and for different molecular-orbital expansions. The results of both types of calculations are summarized in Table II for the two nearest-neighbor CO distances found in the $(\sqrt{3}\times\sqrt{3})$ and $(2\sqrt{3}\times 2\sqrt{3})$ structures, namely 4.35 and 3.29 Å. The results for the interaction matrix elements are rather similar for the two procedures, which reflects the small influence of self-consistency due to the lack of charge rearrangement upon interaction of two CO molecules. This result justifies the use of the simpler approach based on the semiempirical formulas. A closer inspection of Table II reveals some interesting results, which are schematically illustrated in Fig. 9. The two components of the 1π orbital are no longer degenerate for two interacting CO molecules. One part establishes a π-type interaction, the other part a σ-type interaction, of which the latter is by far the larger one [Fig. 9(a)]. The magnitude of the inter-σ interactions (4σ-4σ or 5σ-5σ) is intermediate between the two interaction channels of the 1π orbitals. The 5σ interaction [Fig. 9(c)] is a factor of 2.5 larger than the 4σ interaction. This is due to the composition of the molecular orbitals in terms of atomic orbitals. The 4σ consists of about 60% oxygen atomic orbitals which are more contracted (higher Z) than the carbon orbitals, which make up almost 80% of the 5σ molecular orbital of free carbon monoxide. Finally, we have to consider the interaction between π and σ orbitals indicated in Fig. 9(b). It is already clear from the schematic drawing that the σ-π interaction is at least as large as the 5σ-5σ interaction. In fact, the calculations indicate that it is larger by 10% (see Table II). We will see that this σ-π hybridization interaction becomes important in order to properly describe the dispersion of a CO layer bound to a transition-metal surface.

Figure 10(a) presents the results for the $(2\sqrt{3}\times 2\sqrt{3})$ structure assuming a free CO layer. We have used the experimentally known ionization potentials of free CO as orbital energies of the isolated molecule. The bandwidths are 1.6 eV for 5σ, 0.62 eV for 4σ, and 2.1 eV for the 1π derived bands. For the corresponding $(\sqrt{3}\times\sqrt{3})$ structure with a CO-CO spacing of 4.35 Å we find 0.4 eV for 5σ, 0.1 eV for 4σ, and 0.5 eV for the 1π derived bands. The important result is that the calculated bandwidths are smaller than the separations of ionization potentials in the isolated molecule. Therefore, although there is a σ-π overlap in real space, the energy

TABLE II. Interaction parameters for band-structure calculations (SCF-HF stands for self-consistent-field Hartree-Fock).

Overlap, type	3.29, S_{ij}	4.35, S_{ij}	3.29, KS_{ij}	4.35, KS_{ij}	3.29, $W_{\text{SCF-HF}}$	4.35, $W_{\text{SCF-HF}}$
$\langle 4\sigma \mid 4\sigma\rangle$	3.23×10^{-3}	0.34×10^{-3}	0.068 eV	0.004 eV	0.07 eV	0.002 eV
$\langle 5\sigma \mid 5\sigma\rangle$	8.61×10^{-3}	0.87×10^{-3}	0.179 eV	0.008 eV	0.21 eV	0.005 eV
$\langle 1\pi \mid 1\pi\rangle_\pi$	2.28×10^{-3}	0.14×10^{-3}	0.049 eV	0.001 eV	0.04 eV	0.001 eV
$\langle 1\pi \mid 1\pi\rangle_\sigma$	-16.71×10^{-3}	-1.78×10^{-3}	−0.329 eV	0.012 eV	0.36 eV	0.008 eV
$\langle 1\pi \mid 5\sigma\rangle$	-7.88×10^{-3}	-0.79×10^{-3}	0.199 eV	0.009 eV		

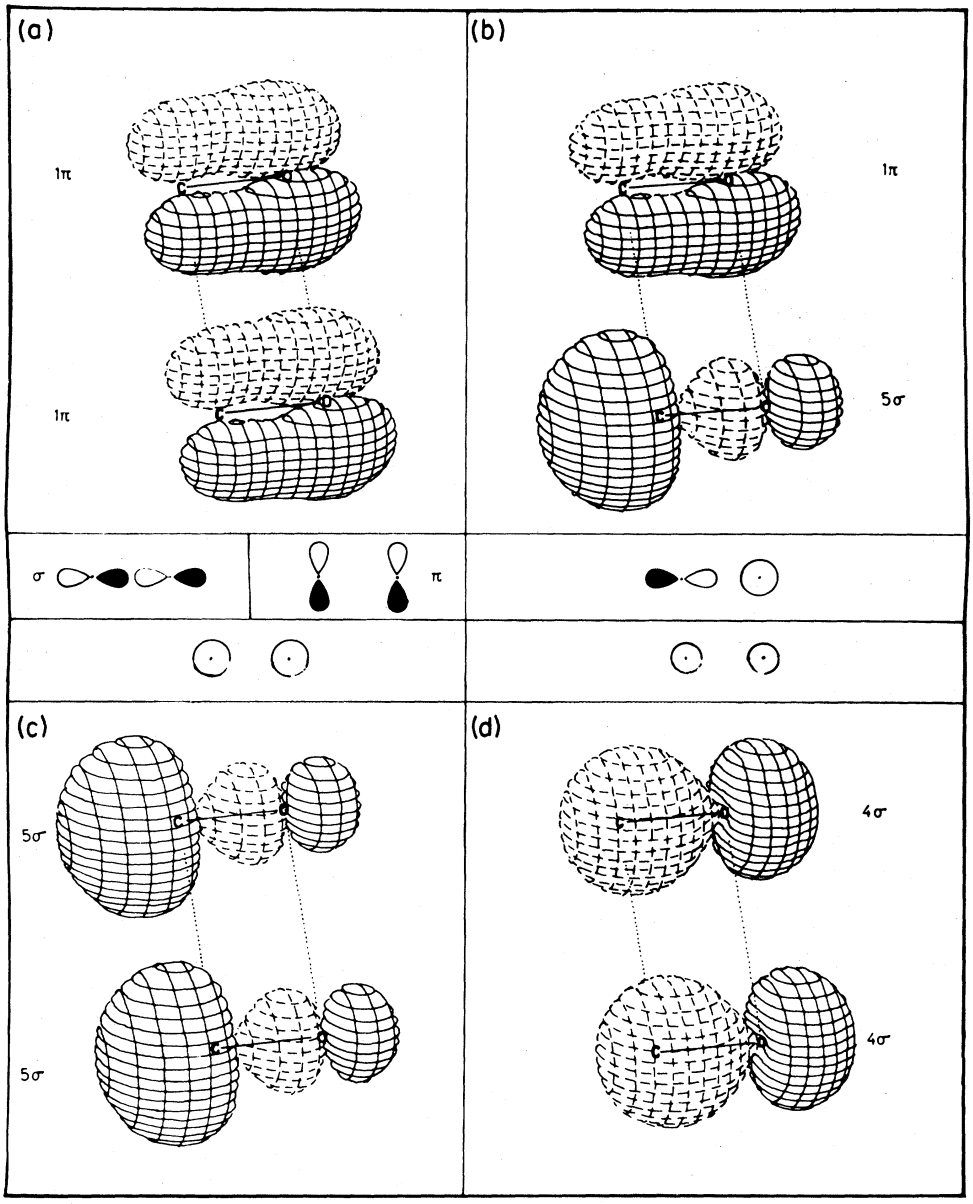

FIG. 9. Three-dimensional orbital plots for two CO molecules ($d_{C\text{-}O}$: 1.15 Å) at an intermolecular separation of 3.29 Å. The plotted lobes enclose 99% of the electrons. Positive lobes are plotted as solid lines, negative lobes as broken lines. The orbital wave functions have been generated using the CNDO formalism: (a) σ-type interaction between 1π orbitals, (b) 5σ-1π hybridization interactions, (c) 5σ-5σ interaction, (d) 4σ-4σ interaction. The schematic orbitals in the center of the figure show an end-on view of the molecular-orbital plots.

separation between the two band systems is too large to significantly influence the dispersion of the bands of an isolated layer of CO molecules.

Before we consider the changes in the CO band structure introduced by the substrate we will briefly discuss the qualitative behavior of the band dispersion shown in Fig. 10(a). The wave functions for this system are two-dimensional Bloch functions so that the wave function at a lattice site specified by the real lattice vector R_1 is related to the wave function at another site R_2 by

$$\psi_k(R_1)=\exp[i\vec{k}\cdot(\vec{R}_1-\vec{R}_2)]\psi_k(R_2)\ ,$$

where $\exp[i\vec{k}\cdot(\vec{R}_1-\vec{R}_2)]$ gives the phase difference

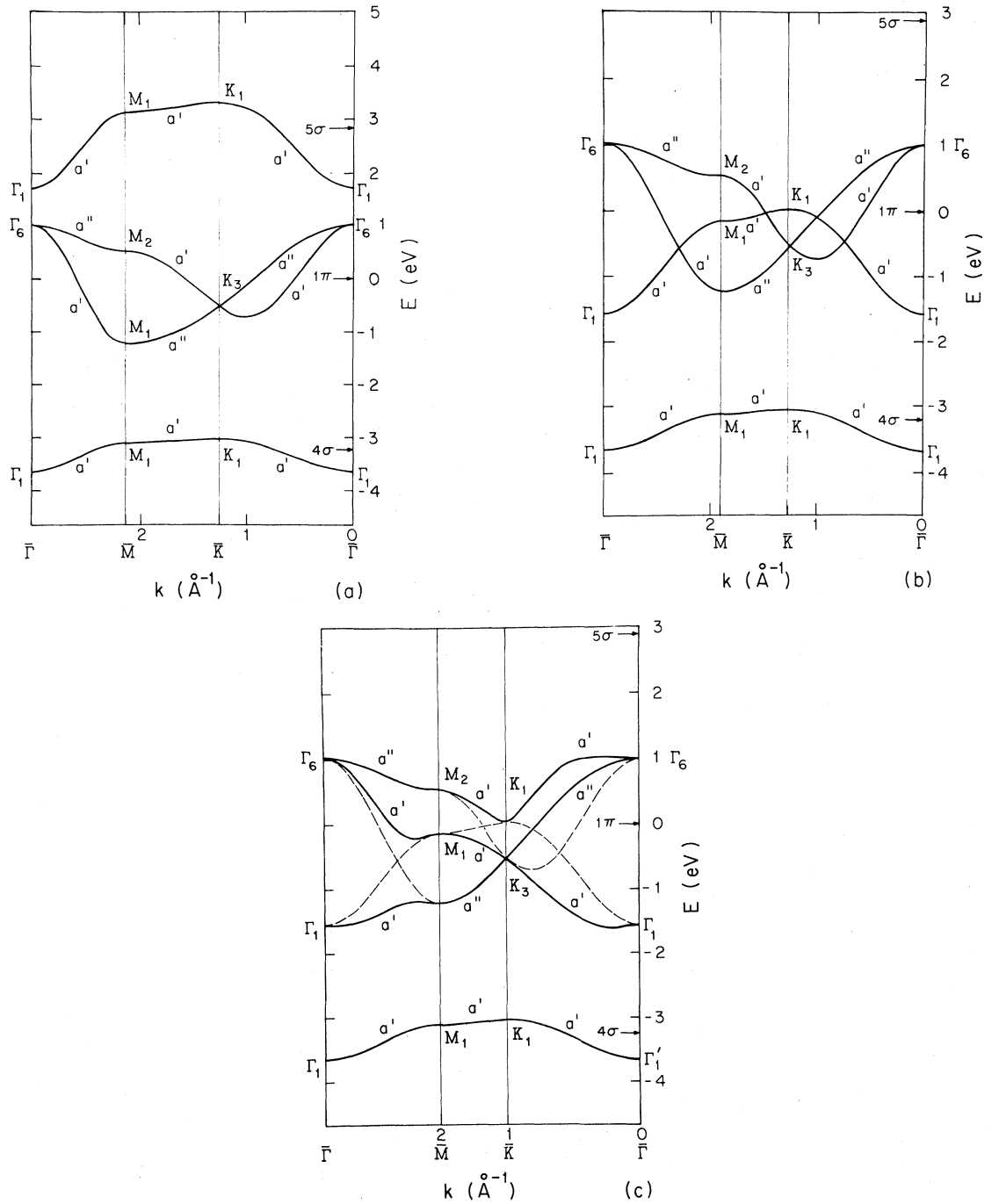

FIG. 10. Calculated electron energy bands for a hexagonal overlayer of free CO molecules. (a) Experimental ionization potentials of the three outer levels of free CO are used to determine the noninteracting CO energy levels (see right-hand side). (b) Same as (a) with the 5σ ionization potential shifted 0.5 eV below the 1π ionization potential. The 5σ-1π hybridization is neglected. (c) Same as (b) with the 5σ-1π hybridization interaction turned on. The arrows mark the free CO ionization potentials in each figure.

between the two sites for a state specified by the wave vector k. We can easily illustrate the qualitative features of the dispersion by plotting schematically the real parts of the tight-binding wave functions in real space for values of k corresponding to high-symmetry points in reciprocal space. Figure 11(a) shows the real- and reciprocal-space unit cells for the hexagonal structure being considered. The

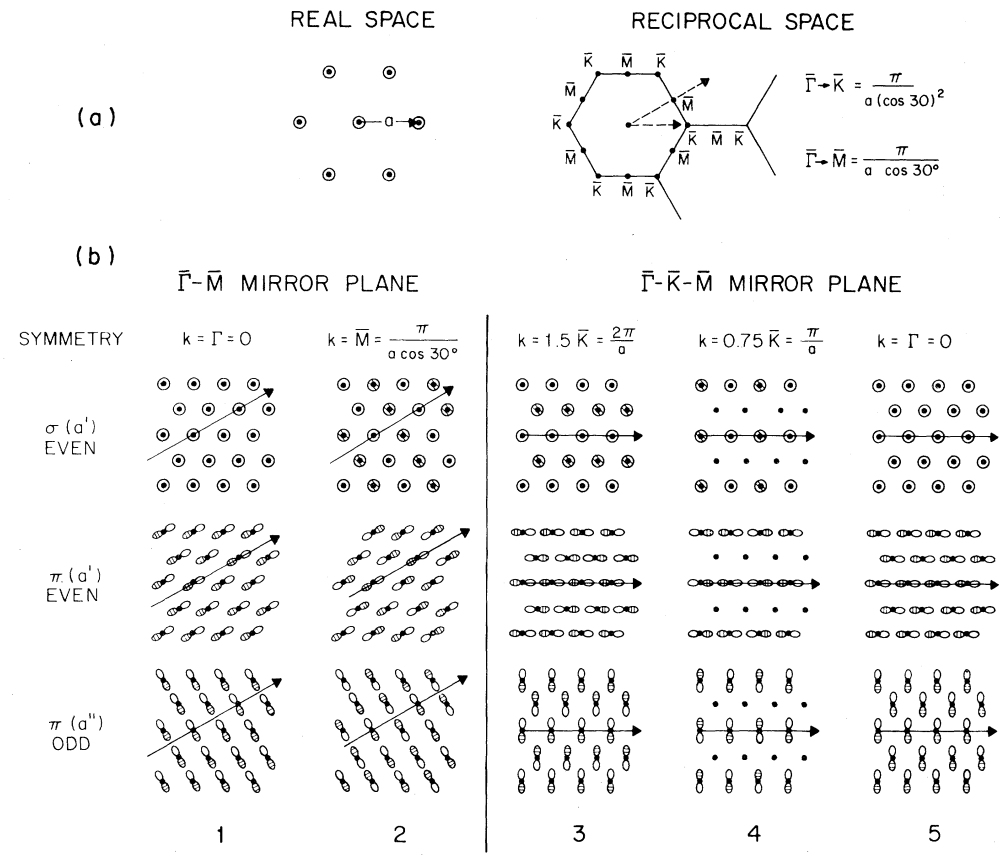

FIG. 11. Schematic representation of wave functions (real part) for a hexagonal CO overlayer: (a) real and reciprocal lattices of hexagonal structure, (b) real part of wave functions for σ and π states at various values of $\vec{k}$. The arrows indicate the direction of $\vec{k}$.

real and reciprocal lattices have two mirror planes, one along the line $\bar{\Gamma}\bar{M}\bar{\Gamma}$ (reciprocal space) and the other along the line $\bar{\Gamma}\bar{K}\bar{M}\bar{K}$. These two mirror planes are shown by the dashed lines on the reciprocal lattice. The wave functions along these lines will be even (a') or odd (a'').

Figure 11(b) illustrates phases of a σ and the two π states at four different values of $\vec{k}$. The two left-hand-side columns are for the $\bar{\Gamma}\rightarrow\bar{M}$ mirror plane while the three right-handed columns are for the $\bar{\Gamma}\bar{K}\bar{M}$ mirror plane. At $\bar{\Gamma}$ ($k=0$) all of the wave functions at the different lattice sites are in phase. This results in a strongly bonding configuration for the σ state (top row), but an antibonding configuration for both π states because the individual π functions change sign about the molecular axis. The π functions have been chosen in columns 1 and 5 so that one is even and one odd with respect to the specific mirror planes. It is easy to see from the pictures in column 1 that the odd and even π states are degenerate at $\bar{\Gamma}$. Therefore, at $\bar{\Gamma}$ we have a strongly bonding σ band and a degenerate antibonding π band.

In the $\bar{\Gamma}$ to $\bar{M}$ mirror plane k increases from zero at $\bar{\Gamma}$ to $\pi/(a\cos30°)$ at the zone boundary ($\bar{M}$). The second column shows the wave functions at $\bar{M}$ where the arrow indicates the direction of $\vec{k}$. All rows of atoms perpendicular to $\vec{k}$ have the same phase but each row has a phase change of π. The result for the σ states is that each atom is surrounded by four atoms of opposite phase (antibonding) and two bonding atoms. The σ bands, therefore, disperse upward from $\bar{\Gamma}$ to $\bar{M}$. In contrast the even π state is strongly bonding since each lobe of the molecular π orbitals sees only bonding nearest neighbors. The even π band disperses downward from $\bar{\Gamma}$ to $\bar{M}$ with the largest difference that will be seen in the π bands. The odd π state at $\bar{M}$ is just slightly more bonding than the π state at $\bar{\Gamma}$ since the overlap of the lobes in a line perpendicular to $\vec{k}$ is antibonding but the overlap between these lines of atoms is bonding. Thus we have explained the qual-

itative features of the dispersion in the $\bar{\Gamma}$ to $\bar{M}$ direction shown in Fig. 10(a).

In the $\bar{\Gamma}\,\bar{K}\,\bar{M}$ direction the wave-function pictures are slightly more complicated because $\bar{\Gamma}\bar{K}$ is not an integral multiple of the row spacing in this direction. The rows of lattice sites perpendicular to the $\bar{\Gamma}\,\bar{K}$ direction are separated by $a/2$. Therefore, we have shown the phase of the wave functions at $k=0.75\bar{k}_{\bar{\Gamma}\bar{K}}=\pi/a$ and at $1.5\bar{k}_{\bar{\Gamma}\bar{K}}=2\pi/a$. $1.5\bar{k}_{\bar{\Gamma}\bar{K}}$ is the $\bar{M}$ point in the extended-zone scheme. Column 5 shows (again) the phases of the σ and π wave functions at $\bar{\Gamma}$. We have now used a different representation of the π functions so that one is even and the other odd with respect to this mirror plane. At $k=0.75\bar{k}_{\bar{\Gamma}\bar{K}}$ each row of lattice sites perpendicular to k is out of phase with the adjacent row by $\pi/2$ so that the amplitude of the phase is $+1, 0, -1, 0, +1$, etc. The sites with zero phase are shown as dots. The σ state at $0.75\bar{k}_{\bar{\Gamma}\bar{K}}$ is antibonding with approximately the same energy as the σ band at $\bar{M}$. The even π band becomes bonding with two nearest-neighbor sites being in phase while the odd π state is basically nonbonding with respect to nearest-neighbor overlap. At $k=1.5\bar{k}_{\bar{\Gamma}\bar{K}}$ the σ state is at approximately the same energy as at $k=0.75\bar{k}_{\bar{\Gamma}\bar{K}}$. At both values of k there is an excess of two antibonding nearest neighbors. The even π band becomes more antibonding at $k=1.5\bar{k}_{\bar{\Gamma}\bar{K}}$. Notice that the wave functions of the π bands at $k=1.5\bar{k}_{\bar{\Gamma}\bar{K}}$ are the same as at $k=\bar{k}_{\bar{M}}$ (column 2) if you rotate the picture by 30° and change the symmetry. The symmetry is different because the $\bar{\Gamma}\bar{M}$ mirror plane is different from the $\bar{\Gamma}\,\bar{K}\,\bar{M}$ mirror plane. Again this simple picture predicts the correct band topology. The σ band disperses upwards from $\bar{\Gamma}$ to $\bar{K}$ with the energy at $k=0.75\bar{k}_{\bar{\Gamma}\bar{K}}$ approximately equal to the energy at $k=1.5\bar{k}_{\bar{\Gamma}\bar{K}}$. The π band disperses downward as k goes from $\bar{\Gamma}$ to $\bar{K}$. At $k=0.75\bar{k}_{\bar{\Gamma}\bar{K}}$ the even band is more bonding than the odd band, but at $k=1.5\bar{k}_{\bar{\Gamma}\bar{K}}$ the odd band is strongly bonding while the even π band becomes more antibonding.

The two-dimensional band structure for an isolated CO layer in Fig. 10(a) is not expected to reproduce many of the features seen experimentally in the CO/Co system, because the CO is not bonded to a substrate in this model. The bonding of the CO to the cobalt substrate will change the wave functions and consequently induce shifts in the energy-level scheme. As explained in the Introduction the CO bonds to the metal primarily through the CO 5σ level causing this energy level to drop in energy with respect to the other CO valence levels. We made a first-order attempt to calculate the effect of the substrate bond upon the CO band structure by using CO gas-phase wave functions with the 5σ ionization potential shifted relative to the 1π and 4σ ionization potentials to correspond to the energy separations observed on the surface.[1] Figure 10(b) shows the calculated band structure of Fig. 10(a) with the 5σ energy shifted to lie 0.5 eV below the 1π level. In this figure there is no σ-π interaction included.

Figure 10(b) shows that the 5σ and 1π bands will overlap in energy for CO on the surface due to the relative drop in the 5σ ionization potential caused by the bonding to the substrate. The σ-π interaction will cause the bands with the same symmetry to mix, thereby producing hybridization gaps. The only symmetry element along the lines in Fig. 10 in the two-dimensional Brillouin zone is a mirror plane so that bands are either odd (a'') or even (a') [see Fig. 10(b)]. Consider as an example the $\bar{\Gamma}$ to $\bar{K}$ direction. The even (a') 5σ band disperses upward from $\bar{\Gamma}$ toward $\bar{K}$ crossing the odd and even π bands, which disperse downward from $\bar{\Gamma}$. The even σ and π bands will hybridize forming a gap in the even bands. Figure 10(c) shows the resulting band structure calculated with the σ-π interaction turned on. The even σ and π bands also cross in the $\bar{\Gamma}$ to $\bar{M}$ and $\bar{M}$ to $\bar{K}$ directions.

The even bands in the 1π-5σ region are now no longer pure π or σ. For example, the bottom even band going from Γ_1 to K_3 in Fig. 10(c) is a band with mixed σ-π character. At Γ_1 it is pure σ and at K_3 it is pure π, but in between $\bar{\Gamma}$ and $\bar{K}$ this band has a continuously changing orbital character. This band mixing makes it impossible to uniquely define a π or σ bandwidth. The data listed in Table I for the experimental and theoretical bandwidth is Γ_1 to K_3 for the 5σ band and Γ_6 to K_3 for the 1π band. The reason that this definition of the bandwidth has been used is that the doubly degenerate K_3 point is easy to determine experimentally. Adopting this definition of the bandwidths gives an accurate description of the π band because the Γ_6 and K_3 points are pure π in character. In contrast, this definition always underestimates the σ-character bandwidth because the K_1 point lies above the K_3 point and is pure σ in character.

Figures 12 and 13 show a comparison of the theoretical calculations and experimental data for the two CO lattices observed experimentally. The overall agreement is surprisingly good considering the simplicity of the calculation. In particular, the changes in the bandwidths between the two structures are remarkably well reproduced. The 4σ bandwidth increases from 0.15 to 0.48 eV experimentally in going from the low-coverage $(\sqrt{3}\times\sqrt{3})R30°$ structure to the higher coverage $(2\sqrt{3}\times 2\sqrt{3})R30°$, compared to 0.1–0.6 eV theoretically. The calculated 1π bandwidth from $\bar{\Gamma}$ to $\bar{K}$ changes from 0.4 to

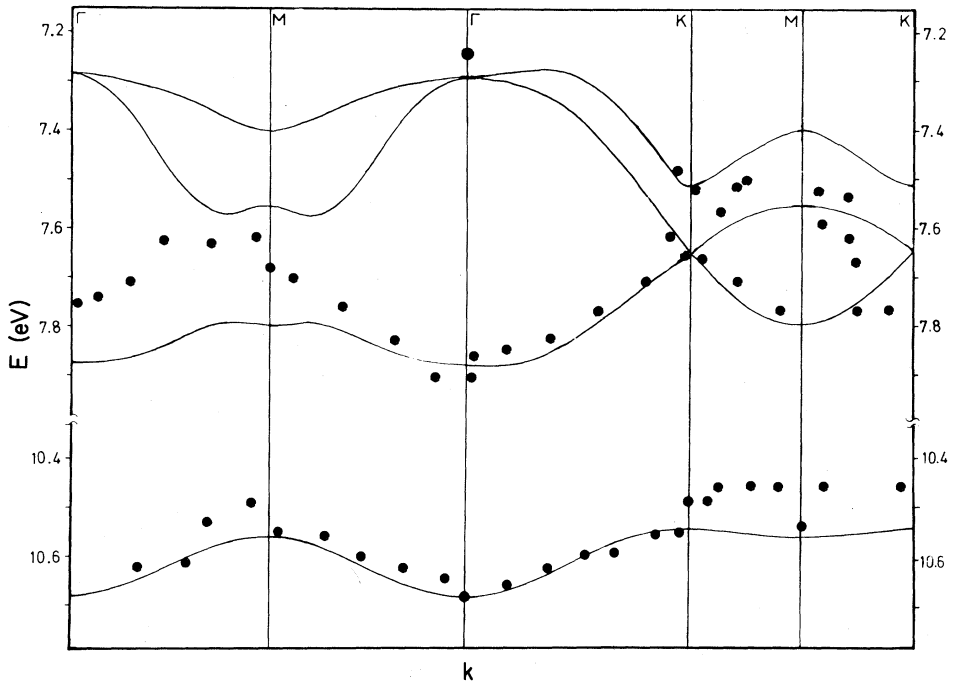

FIG. 12. Comparison between calculated and measured band dispersions for the $(\sqrt{3}\times\sqrt{3})$ structure. A few extra data points, mainly from the 1π levels, have been added as compared with Fig. 3.

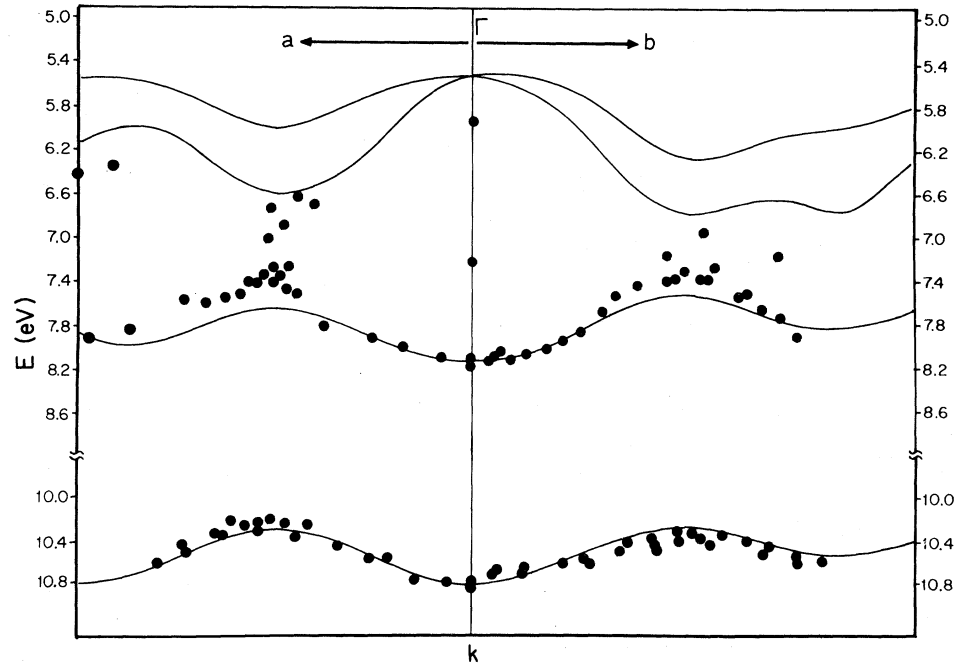

FIG. 13. Comparison between calculated and measured band dispersions for the $(2\sqrt{3}\times 2\sqrt{3})$ structure. The measurements and calculations were made along lines *a* and *b* shown in the inset in Fig. 4.

1.6 eV while the experimental data shows a change from 0.35 to 1.1 eV. Likewise, the experimental and theoretical 5σ bandwidths for the two structures are in good agreement. The last column of Table I lists the ratio of the 5σ and 1π bandwidths compared to the 4σ bandwidths. The theoretical and experimental ratios for the high-density CO layer agree very well. There is a larger disagreement for the low-coverage phase but the relative experimental errors are large for the small dispersion seen in this case. Note that the dispersion calculations for the high-coverage phase (Fig. 13) were made along lines *a* and *b* in Fig. 4 to match the experimental data.

We have not included in our calculations any change in the CO wave functions caused by the presence of the Co surface. The simplest way to incorporate these effects into our calculational scheme is to do a cluster calculation for a linear transition-metal CO cluster,[24] then "cut off" the CO from the metal and renormalize the CO wave functions. This procedure leads to some interesting qualitative changes in the relative bandwidths of the 4σ- and 5σ-derived bands. When the CO molecule bonds to the transition metal the 4σ and the 5σ CO orbitals mix. That is, the 4σ level acquires more diffuse carbon character, while the 5σ admixes more contracted oxygen character. A consequence of this mixing is that for a given CO-CO spacing in the hexagonal overlayer the 4σ bandwidth increases while the 5σ bandwidth decreases. Therefore, the band dispersion calculated with metal-CO wave functions would not agree as well with the measured bands as it does with the calculation based on free CO wave functions. This fact should not be interpreted as implying that there is no mixing of the gas-phase 4σ and 5σ levels upon bonding of CO to a transition metal. Instead it illustrates the simplicity of our calculational scheme. The intensity of the 5σ shape resonance in adsorbed CO compared to the 4σ intensity, as well as the sign of the work-function change, indicate that there is 4σ-5σ mixing in the adsorbed CO (Ref. 25) (also see Appendix).

Another aspect of the experimental spectra that we wish to discuss in this section is the splitting of the π bands at $\bar{\Gamma}$ that is suggested by the broad feature observed in Fig. 7. Although, as mentioned above, the bands are degenerate at $\bar{\Gamma}$ in an isolated CO layer the bands may split due to the incommensurability of the overlayer with the Co substrate in the high-coverage phase. This reduces the global symmetry such that the symmetry is less than C_{3v} even at $\bar{\Gamma}$. For the commensurate $(\sqrt{3}\times\sqrt{3})$ structure on the substrate the symmetry at $\bar{\Gamma}$ reduces from C_{6v} in the isolated layer to C_{3v}. All other symmetry points have reduced symmetry. For example, $\bar{K}$ no longer has a threefold axis so that the levels can split at this point even in the commensurate layer. The observed splitting at $\bar{\Gamma}$ is rather large, 1.1 ± 0.3 eV. In order to check whether this magnitude is compatible with theoretical predictions we have carried out a calculation[24,26] of the simplest imaginable bridge-bonded site, namely two neutral metal atoms set apart by the bulk nearest-neighbor distance and bridged by a CO molecule with its axis perpendicular to the metal-metal separation. Now the two π levels split due to the fact that one π component can form a σ-type interaction with the two metal atoms, while the other component can only interact through the π channel. For computational convenience available wave functions for Ni-substrate atoms were used.[24] The calculated splitting is 1.9 eV, which should represent an upper limit to the observable value due to the chosen geometry. Rosen *et al.*[27] have calculated the splitting in the π levels for a bridge-bonded $(Ni)_2CO$ system in a self-consistent Hartree-Fock-Slater calculational scheme. Their calculated splitting was only 0.8 eV.

Finally, we should discuss briefly the shift in binding energy between the two phases of CO. Consider the example the 4σ level of the low- and high-coverage phases. The weighted average (over the bandwidth) of the 4σ binding energy referenced to the vacuum level is 16.5 and 16.9 eV for the low- and high-density CO layers, respectively. We have used the measured work function to determine these binding energies. The high-density phase has approximately 0.4 eV higher binding energy than the low-density phase, presumably because of the reduction in the metal screening due to the weaker coupling between the CO and the metal. A detailed analysis of these binding energies would have to include the changes in the intralayer screening as well.

V. CONCLUSIONS

We have measured the two-dimensional energy-band dispersion for two hexagonal overlayers of CO on the Co(0001) surface. The CO lattice spacing changed from 4.35 Å in the low-coverage commensurate $(\sqrt{3}\times\sqrt{3})R\,30°$ structure to 3.29 Å in the high-coverage $(2\sqrt{3}\times2\sqrt{3})R\,30°$ incommensurate structure. The CO bandwidths increase by approximately a factor of 3 as the density increases 75%. The magnitude and shape of the measured dispersion as a function of CO-CO spacing can be explained in a semiquantitative fashion by a tight-binding calculation utilizing gas-phase CO wave functions if the 5σ ionization potential is artificially shifted to account for the bonding shift induced by coordination of the CO to a transition metal. The shifted 5σ level forms a band which hybridizes with the 1π bands. This hybridization is important to

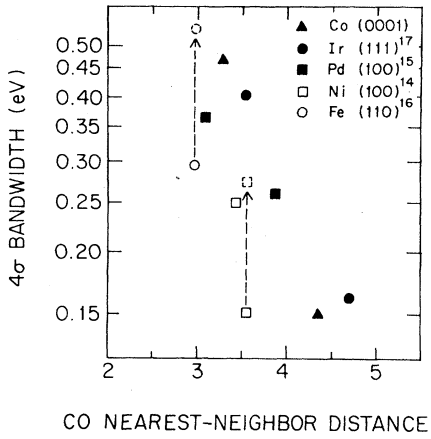

FIG. 14. Comparison of experimental 4σ bandwidths vs CO nearest-neighbor distance for various CO chemisorption systems. The dashed lines indicate corrections based on the different geometries of the Ni and Fe systems (fewer nearest neighbors than the other hexagonal overlayers). The bandwidths are plotted on a log scale.

understand the dispersion and photoemission properties of ordered CO on a surface.

The implication of the data and theory is that the band dispersion is primarily a consequence of direct CO-CO interactions and not due to indirect interactions through the substrate. Figure 14 shows a compilation of the measured 4σ bandwidths for ordered CO layers on various substrates as a function of the CO-CO spacing. The dashed lines show a first-order (tight-binding) correction of the $c(2\times2)$ square CO structure on Ni(100) and the $p(1\times2)$-Fe(110) structure to correspond to an equivalent hexagonal structure.[28] All of the other structures are either quasihexagonal or real hexagonal overlayers. The data points, especially for the true hexagonal overlayers (Ir and Co), follow an exponential dependence on the nearest-neighbor distance with a decay length of ~ 1.3 Å. This strongly supports the conclusion that the 4σ dispersion is caused by direct CO-CO overlap. The only direct experimental observation which depended upon the coordination geometry of the overlayer with respect to the substrate was the splitting of the degenerate 1π level at $\bar{\Gamma}$ in the incommensurate structure.

ACKNOWLEDGMENTS

We would like to thank the staff at the Synchrotron Radiation Center, University of Wisconsin—Madison, for their support. This work was supported by U. S. Office of Naval Research and the Synchrotron Beam Line facility was constructed and maintained by the Materials Reseach Laboratory of the University of Pennsylvania under the National Science Foundation Grant No. DMR-79-23647. H.J.F. would like to acknowledge the support of the Deutsche Forschungemeinschaft.

TABLE III. Charge densities in free and coordinated CO. $d_{C\text{-}O}$: 1.15 Å; $d_{Ni\text{-}CO}$: 1.82 Å.

	CO	NiCO	Δ
C	−0.0483	+0.0862	+0.1345
O	+0.0483	−0.0986	−0.1469
CO		−0.0124	−0.0124
Ni		+0.0124	+0.0124

APPENDIX: SHAPE RESONANCES

Figure 15 shows plots of the photoionization cross sections for the 4σ and 5σ-1π levels as a function of photon energy for the low- and high-coverage phases of CO on Co(0001). It is known theoretically[29–35] and experimentally[19,36,37] that the energy dependence of the cross section of these levels in the free molecule is dominated by a molecular shape resonance. Allyn *et al.*[38] have shown that this feature persists when the molecule is adsorbed onto a surface and Loubriel and Plummer[25] have demonstrated that the resonance exists in transition-metal carbonyl complexes. This resonance has σ symmetry[29,30] and has been used to identify the symmetry of ion states.[19] The resonance emission for the excitation from the 4σ level is directed out of the oxygen end of the molecule and has been used to determine that CO is bound carbon end down to the surface. Calculations for the free CO molecule indicate that the resonance emission from the 5σ level should be primarily out of the carbon end.[25,39]

The cross section versus photon energy for all CO adsorption systems except CO on Cu(111) (Refs. 1 and 38) shows a stronger resonance in the combined 5σ-1π peak than in the 4σ peak, which contradicts the predictions for gas-phase CO. This increased resonance emission is not likely to result from 1π emission since the 1π does not couple to the resonant state for free CO (Ref. 36) and the 1π level is not significantly perturbed by bonding to the substrate. It is also easy to rule out backscattering from the substrate because the resonance is basically the same for the commensurate and incommensurate structures (Fig. 15). The unresolved question is why the resonant emission from the 5σ level is so intense in normal emission for chemisorbed CO.

The data in Fig. 15 have been normalized to the coverage as determined from the LEED patterns, so the intensity scale is proportional to differential

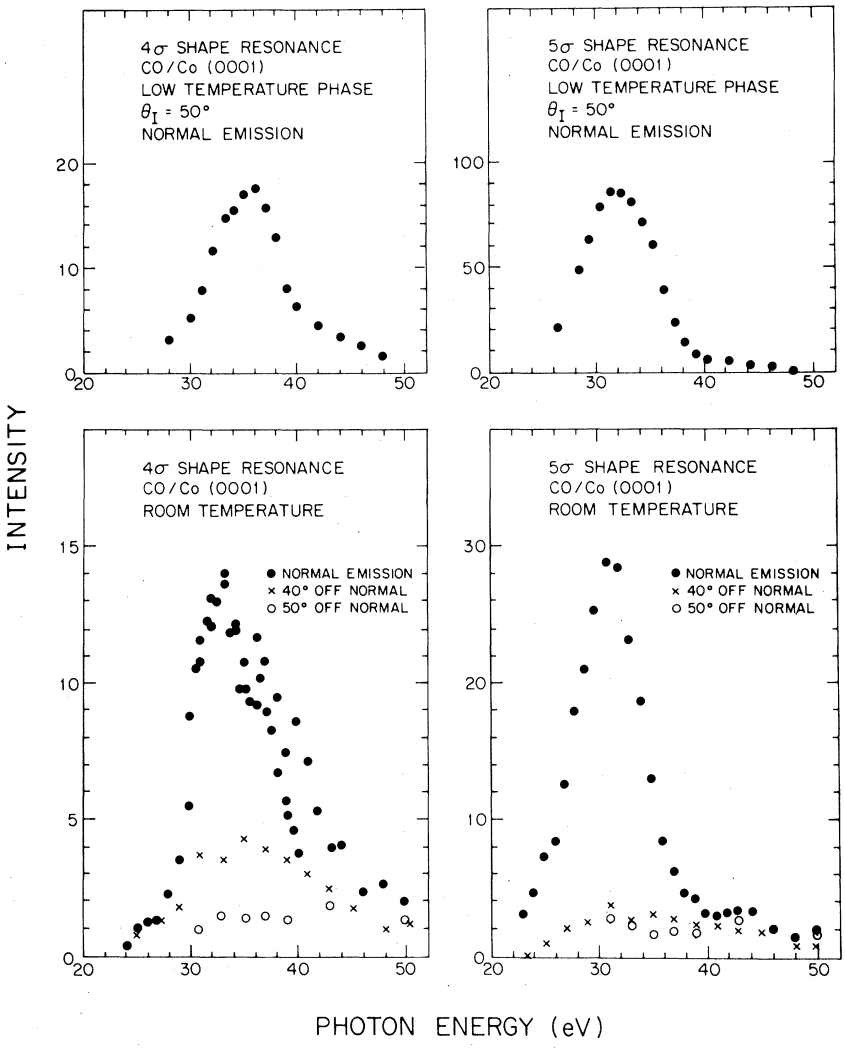

FIG. 15. Angle-resolved photoionization cross sections from the 4σ and 5σ-1π levels of CO/Co(0001).

cross sections per molecule. The maximum intensity in the 4σ resonance goes from ~ 14 at room temperature to ~ 18 at low temperature. This $\sim 25\%$ change is probably not significant because the two sets of data were accumulated several days apart and factors such as movement in the synchrotron beam orbit or changes in the multiplier gain could produce this small change. For example, there are two sets of data shown in the room-temperature 4σ resonance plot showing up to 25% variation in calibration. In contrast, the emission from the 5σ-1π level goes from a maximum of 29 at room temperature to ~ 90 at low temperature, a threefold increase in the normal emission. This implies that the 5σ resonant emission out of the oxygen end of each CO molecule has increased by 200% in the high-coverage structure compared to the low-coverage structure.

Loubriel and Plummer[25] have proposed a simple picture of the resonant emission which qualitatively explains the increased 5σ resonant emission out of the oxygen end of the molecule. Briefly, these authors determine the overlap between the dominant radial part of the resonant wave function, namely an f wave with $l=3$ and $m=0$ and the initial state, e.g., a 4σ or 5σ orbital. The plot of this overlap as a function of electron position makes it possible to determine which spatial regions of the initial state contribute to the resonance excitation. Since the amplitude of the resonance is determined by the dipole matrix element

$$|\langle \psi_f | \vec{r} | \psi_i \rangle|^2 , \tag{A1}$$

with ψ_f and ψ_i the final and initial states, a strong signal is expected if the overlap plot exhibits a large dipole moment. Loubriel and Plummer[25] clearly showed that most of the overlap occurs in the oxygen side for the 4σ initial state with only small contributions on the carbon side. On the other hand, the 5σ has about as much overlap on the carbon as on oxygen and therefore exhibits no strong dipole moment. Upon adsorption the 5σ wave functions and final state will change. Therefore, the resonance behavior of the 5σ level drastically changes when CO is bound to a transition-metal atom. Following these lines of thought we are able to qualitatively estimate what happens.

Upon adsorption the 5σ orbital is shifted towards the 1π orbital with respect to free CO because of the interaction with metal orbitals. This stabilization of the 5σ orbital decreases the 4σ-5σ energy separation considerably. The consequence is a remixing of the 4σ and 5σ orbitals (or better, of all σ orbitals) of bound CO. This leads to a redistribution of electrons on CO toward the oxygen. In other words, the occupied orbitals gain more oxygen character, which is a "more natural" electron distribution than in free CO where the electron distribution is such that the carbon is negative and the oxygen is positive.[40] The electron redistribution introduces more oxygen character also in the 5σ orbital and hence leads to more oxygen character in the above-discussed overlaps. At the same time this induces a strong dipole moment into this overlap distribution allowing for a large shape resonance intensity.

In order to substantiate the qualitative analysis on charge distributions we have carried out self-consistent-field molecular-orbital (SCF-MO) calculations on a linear metal-CO cluster, namely Ni-CO. We employ a semiempirical CNDO Hamiltonian that has been fit to reproduce Hartree-Fock (*ab initio*) results on molecules. We augment the results by means of a configurational interaction treatment including the 2400 lowest-lying single and double excited configurations.[41] The charge densities calculated using this method for free CO and Ni-CO on the one-particle and CI level are given in Table III. The calculated charge distribution is consistent with the experimentally determined increase in the work function for CO on transition metals. This explanation of the change in the resonance intensities offers the advantage that one can discuss the shape resonance intensities observed for various substrates as a function of molecule-substrate interactions.[1] As an example, the 5σ resonance for CO/Cu(111) is very weak,[7] which is probably due to the much weaker CO—metal bond. At the same time, the work function decreases instead of increasing upon CO adsorption. The charge distribution on adsorbed CO clearly is a function of several parameters, one of which is the bonding site. As far as the bonding site is concerned a bridge bond usually leads to stronger charge separation on the CO unit compared with linear bonding, with the oxygen carrying the negative charge.[42] This, also, could lead—in line with the above arguments—to a resonance enhancement.

Another parameter that may be important is intermolecular interactions. It is known that intermolecular interactions strongly influence the infrared intensities and frequencies[42] of adsorbed species due to dipole-dipole coupling. Pfnür *et al.*[42] have demonstrated for the $(\sqrt{3}\times\sqrt{3})$ and $(2\sqrt{3}\times 2\sqrt{3})$ phases of CO on Ru(0001) that a shift of approximately 60 cm^{-1} is connected with the phase transition. This type of effect should influence the relative intensities of the 4σ and 5σ shape resonances.

In conclusion, the main mechanisms leading to the increased 5σ resonant emission in the room-temperature phase compared to free CO is due to mixing of σ states upon adsorption. The simplest application of this model would predict that the 4σ emission would decrease as the 5σ emission increases. A comparison of the room- and low-temperature phases in Fig. 15 show that this does not happen; in fact, the 4σ emission is basically unaffected while the 5σ emission changes by a factor of 3. A detailed analysis of the wave functions is necessary for a quantitative comparison. Alternatively, the large increase in the 5σ resonant emission in the low-temperature phase versus room-temperature phase might be caused by multiple metal bonding with a reduction in symmetry of the bonding site, as is already suggested by the observation of the split 1π level at $\bar{\Gamma}$.

---

*Present address: Brown-Boveri Company Research Center, CH-5405 Baden, Switzerland.

[1]See, e.g., E. W. Plummer and W. Eberhardt, Adv. Chem. Phys. 49, 533 (1982) and references therein.

[2]M. E. Bridge, C. M. Comrie, and R. M. Lambert, Surf. Sci. 67, 393 (1977); J. Catal. 58, 28 (1979).

[3]H.-J. Freund and G. Hohlneicher, Ber. Bunsenges. Phys. Chem. 83, 100 (1979).

[4]H. Papp, Habilitationsschrift, University Erlangen-Nuernberg, 1979 (unpublished).

[5]J. C. Fuggle, T. E. Madey, M. Steinkelberg, and D. Menzel, Surf. Sci. 52, 521 (1975).

[6]E. D. Williams and W. H. Weinberg, Surf. Sci. 82, 93 (1979).

[7]G. Broden, T. Rhodin, C. Brucker, R. Benbow, and Z. Hurych, Surf. Sci. 59, 593 (1979).

[8]See, e.g., (a) C. M. Comrie and W. H. Weinberg, J. Chem. Phys. 64, 250 (1976); (b) H. Conrad, G. Ertl, J. Kueppers, and E. E. Latta, Surf. Sci. 57, 475 (1976); (c) G. Ertl, M. Neumann, and K. M. Streit, *ibid.* 64, 393 (1977); (d) J. Pritchard, *ibid.* 79, 231 (1979); (e) J. C. Campuzano, R. Dus, and R. G. Greenler, *ibid.* 102, 172 (1981); (f) J. C. Tracy and P. W. Palmberg, J. Chem. Phys. 51, 4852 (1969).

[9]B. P. Tonner and E. W. Plummer, Nucl. Instrum. and Methods 177, 153 (1980).

[10]C. L. Allyn, T. Gustafsson, and E. W. Plummer, Rev. Sci. Instrum. 49, 1197 (1978).

[11]F. J. Himpsel and D. E. Eastman, Phys. Rev. B 20, 3217 (1979); 21, 3207 (1980).

[12]J. C. Bertolini and B. Tardy, Surf. Sci. 102, 131 (1981).

[13]K. A. Prior, K. Schwaha, and R. M. Lambert, Surf. Sci. 77, 193 (1978).

[14]K. Horn, A. M. Bradshaw, and K. Jacobi, Surf. Sci. 72, 719 (1978).

[15]K. Horn, A. M. Bradshaw, K. Hermann, and I. P. Batra, Solid State Commun. 31, 257 (1979).

[16]E. S. Jensen and T. Rhodin, J. Vac. Sci. Technol. 18, 470 (1981).

[17]C. W. Seabury, E. S. Jensen, and T. Rhodin, Solid State. Commun. 37, 383 (1981).

[18]D. Heskett, F. Greuter, H.-J. Freund, and E. W. Plummer, J. Vac. Sci. Technol. 20, 623 (1982).

[19]T. Gustafsson, Surf. Sci. 94, 593 (1980).

[20]S. P. Weeks and E. W. Plummer, Solid State Commun. 21, 695 (1977); alternatively, a fraction of spectrum with dominating 5σ emission can be subtracted from a spectrum with dominating 1π emission, in order to minimize the adsorbate emission at the 5σ binding energy.

[21]H. Jones, *Theory of Brillouin Zones* (North-Holland, Amsterdam, 1975).

[22](a) J. Callaway, *Quantum Theory of the Solid State* (Academic, New York, 1974); (b) B. J. Ransil, Rev. Mod. Phys. 32, 245 (1960).

[23]J. A. Pople and D. L. Beveridge, *Approximate Molecular Orbital Theory* (McGraw-Hill, New York, 1970).

[24]H.-J. Freund and G. Hohlneicher, Theor. Chim. Acta 51, 145 (1979); D. Saddei, H.-J. Freund, and G. Hohlneicher, Surf. Sci. 95, 527 (1980).

[25]G. Loubriel and E. W. Plummer, Chem. Phys. Lett. 64, 234 (1979).

[26]H.-J. Freund (unpublished); F. J. Himpsel, N. Schwentner, and E. E. Koch, Phys. Status Solidi B 71, 615 (1975).

[27]A. Rosen, E. J. Baerends, and D. E. Ellis, Surf. Sci. 82, 139 (1979).

[28]The measurement of dispersion for the $c(2\times2)$CO on Ni(100) was along the $\bar{\Gamma}$ to $\bar{X}$ direction (Ref. 14). A nearest-neighbor tight-binding calculation shows that the dispersion in this direction is half the magnitude of the dispersion in a hexagonal layer along the $\bar{\Gamma}$ to $\bar{M}$ direction for the same CO-CO spacing.

[29]J. L. Dehmer and D. Dill, J. Chem. Phys. 65, 5327 (1976).

[30]J. W. Davenport, Phys. Rev. Lett. 36, 945 (1976).

[31]N. Padial, G. Csanak, B. V. McKoy, and P. W. Langhoff, J. Chem. Phys. 69, 2992 (1978).

[32]J. W. Davenport, J. Vac. Sci. Technol. 15, 433 (1978).

[33]J. L. Dehmer, D. Dill, and S. Wallace, Phys. Rev. Lett. 43, 1005 (1979).

[34]F. A. Grimm, T. A. Carlson, W. B. Press, P. Argon, J. O. Thomson, and J. W. Davenport, J. Chem. Phys 72, 3041 (1980).

[35]F. A. Grimm, Chem. Phys. 58, 71 (1980).

[36]E. W. Plummer, T. Gustafsson, W. Gudat, and D. E. Eastman, Phys. Rev. A 15, 2339 (1977).

[37]B. E. Cole, D. L. Ederer, R. Stockbauer, K. Codling, A. C. Parr, E. D. Polliakoff, and J. L. Dehmer, J. Chem. Phys. 72, 6308 (1980).

[38]C. L. Allyn, Ph.D. thesis, University of Pennsylvania, 1978 (unpublished); C. L. Allyn, T. Gustafsson, and E. W. Plummer, Solid State Commun. 24, 531 (1977).

[39]J. W. Davenport, Ph.D. thesis, University of Pennsylvania, 1976 (unpublished).

[40]B. Rosenblum, A. N. Nethercot, Jr., and C. H. Townes, Phys. Rev. 109, 400 (1958). C. A. Burrns, J. Chem. Phys. 28, 47 (1958).

[41]H.-J. Freund and B. Dick (unpublished).

[42]H. Pfnür, D. Menzel, F. M. Hoffman, A. Ortega, and A. M. Bradshaw, Surf. Sci. 93, 431 (1980).